Supercapacitance Performances of Electrodeposited Co(OH)₂ /three-dimensional Graphene Nanocomposite

Wenju Weng[1,2], Ruyi Zou[1], Wencheng Wang[1], Guiling Luo[1], Hui Xie[1], Chunxiao Yin[2], Shaoyu Wang[1] Guangjiu Li[2], Wei Sun[1,]*

[1] Key Laboratory of Functional Materials and Photoelectrochemistry of Haikou, College of Chemistry and Chemical Engineering, Hainan Normal University, Haikou 571158, P R China
[2] Key Laboratory of Sensor Analysis of Tumor Marker of Ministry of Education, College of Chemistry and Molecular Engineering, Qingdao University of Science and Technology, Qingdao 266042, P R China
[*]E-mail: sunwei@hainnu.edu.cn

In this paper an electrodeposited Co(OH)₂ and three-dimensional graphene (3DGR) nanocomposite was directly synthesized on the surface of carbon ionic liquid electrode (CILE) with its supercapacitance performances checked in detail. The structure and morphology of the prepared Co(OH)₂/3DGR nanocomposite was characterized by scanning electron microscopy (SEM), which gave a porous microstructure on the electrode surface. Various electrochemical methods were applied to investigate the electrochemical performances. The results indicated that Co(OH)₂/3DGR nanocomposite possessed a superior specific capacitance of 730.23 mF/cm² at the current density of 5 mA/cm². And 79.83% of the specific capacitance was retained after 3000 cycles at the current density of 20 mA/cm². Owing to its favorable electrochemical performance, Co(OH)₂/3DGR nanocomposite had a great potential application in the fabrication of electrochemical supercapacitors.

1. INTRODUCTION

Graphene (GR) has been received much attentions due to its unique characteristics such as high conductivity, large specific surface, good chemical stability and mechanical properties [1-3], which has been used as capacitor material with high conductivity and excellent cyclic stability [4, 5]. Three-dimensional graphene (3DGR) is constructed from the two-dimensional planar GR nanosheet, which exhibits porous structure, large specific surface area and high electrical conductivity [6, 7]. Cao et al.

[8] synthesized a MoS_2-coated 3DGR network by chemical vapor deposition and used as anode material for the lithium-ion battery. Pseudocapacitive supercapacitors exhibit the advantages such as high-energy storage and cheaper price. However, its poor electrical conductivity decreases the power density [9, 10]. Also these electrode materials appear irreversible phenomenon in a certain degree during the redox process, which influence the stability and cycle life. Recently many references about the construction of composite electrode with GR and pseudocapacitance materials had been reported [11-14]. For example, Gao et al. [15] used electrodeposition method to prepare GR/polyaniline composite, which had the capacitance value of 5.16 F/cm^2 with the retention rate of capacitance as 93% after 1000 cycles. Zhang et al. [16] prepared a one-step electrochemical co-deposition method to prepare GR/polyaniline composite, which gave the maximum capacitance of 1136.4 F/g with the retention rate of the capacitance as 89% after 1000 cycles. Yan et al. [17] reported a simple preparation method of GR-manganese dioxide nanocomposites with good cycling stability and the loss rate of capacitance was only 4.6% after 15000 cycles. Chen et al.[18] synthesized a GR-$Co(OH)_2$ nanocomposite with the specific capacitance of 972.5 F/g as compared to individual GR (137.6 F/g) and $Co(OH)_2$ (726.1 F/g). Electrochemical deposition is a commonly used method to obtain the different structures of $Co(OH)_2$ from Co salt, which is simple in operation and easy to be realized [19-23].

In this paper electrochemical deposition was performed to get 3DGR modified electrode and then nanosized $Co(OH)_2$ was further potentiostatic deposited on the surface of 3DGR. The $Co(OH)_2$/3DGR nanocomposite formed on the electrode surface was characterized by SEM and electrochemical methods were used to test the capacitor performance of nanocomposite.

2. EXPERIMENTAL

2.1 Apparatus

All the electrochemical measurements including cyclic voltammetry (CV) and electrochemical impedance spectroscopy (EIS) were performed by a CHI 660D electrochemical workstation (Shanghai Chenhua Instrument, China). A typical three-electrode system was used for electrochemical experiments, where $Co(OH)_2$/3DGR/CILE (Φ=4.0 mm) acted as the working electrode, Ag/AgCl or Hg/HgO electrode as the reference electrode and platinum electrode as the auxiliary electrode. Scanning electron microscopy (SEM) was performed on a JSM-7100F scanning electron microscope (Japan Electron Company, Japan).

2.2 Reagents

Graphite powder (average particle 30 μm, Shanghai Colloid Chem. Co., China), graphene oxide (GO, Taiyuan Tanmei Co. Ltd., China), 1-hexylpyridinium hexafluorophosphate ($HPPF_6$, Lanzhou Yulu Fine Chem. Ltd. Co., China), lithium perchlorate ($LiClO_4$, Chengdu Kelong Chem. Co., China) and $Co(NO_3)_2 \cdot 6H_2O$ (Sinopharm. Chem. Reagent Ltd. Co., China) were used as received. All
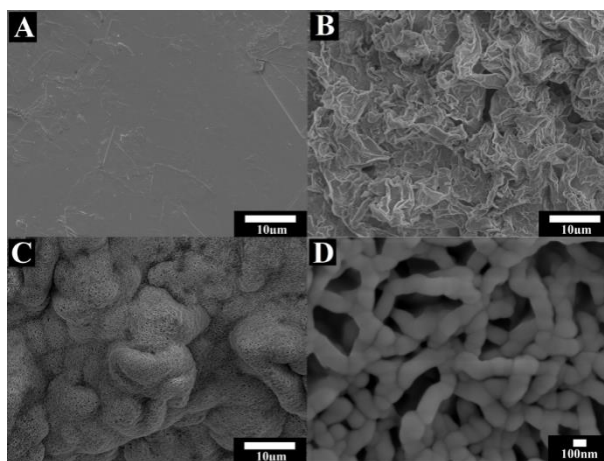
the other chemicals were analytical grade and doubly distilled water was used to prepare the solutions.

2.3 Preparation of the working electrode

Carbon ionic liquid electrode (CILE) was manufactured based on the reference [24] and acted as basal electrode, which was polished on the surface of a weighing paper before used. 3DGR and nanosized $Co(OH)_2$ were electrochemical synthesized directly on the surface of CILE by the following procedure. Firstly CILE was placed in the mixture of 1.0 mg/mL GO and 0.1 mol/L $LiClO_4$ solution with magnetic stirring and N_2 bubbling about 30 min. Then potentiostatic electrodeposition was performed at the potential of -1.3 V for 300 s to get a 3DGR modified CILE. After that 3DGR/CILE was put a 0.1 mol/L $Co(NO_3)_2$ solution with the applied potential of -0.9 V for 300 s to get $Co(OH)_2$/3DGR/CILE.
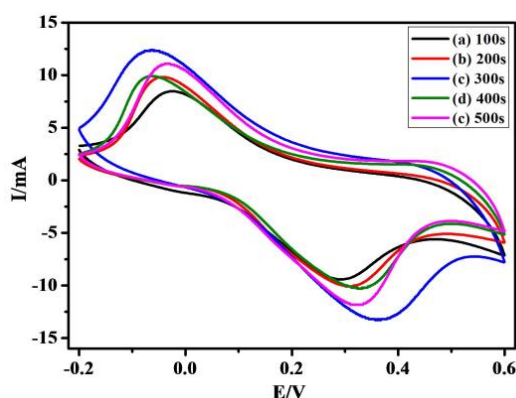
3. RESULTS AND DISCUSSION

3.1 SEM images

Figure 1. SEM images of (A) CILE, (B) 3DGR/CILE, (C) and (D) $Co(OH)_2$/3DGR/CILE with different magnification.

SEM images of CILE (A), 3DGR/CILE (B) and $Co(OH)_2$/3DGR/CILE(C,D) were displayed in Fig.1. CILE displayed a flat and smooth surface, which was due to the high viscosity of ionic liquid (IL) that bound the graphite powder together. After electrochemical reduction of GO on CILE, a disorder and plicate three-dimensional structure could be found on the electrode surface, which was in accordance with the references [25, 26]. Electrochemical reduction can be used for the synthesis of 3DGR directly on the electrode surface with the network formed, which had been explained in detail [27, 28]. As shown in Fig.1 C and D, SEM images of $Co(OH)_2$/3DGR nanocomposite in different magnification exhibited a macroporous structure with nanosized $Co(OH)_2$ displayed as connected and reticular structure, which was uniformly distributed on the surface of 3DGR. This macroporous structure can provide high specific surface area, which is benefit for sufficiently contact of electrolyte

with electrode surface and effectively promote electron transfer rate to electrolyte. The presence of 3DGR can provide a platform for the growth of nanosized $Co(OH)_2$ on its surface. The detail explanation about the synthesis mechanism of $Co(OH)_2$ includes the electrochemical and precipitation reaction with following equations [29]: $NO^{3-} + 7H_2O + 8\ e^- \rightarrow NH_4^+ + 10\ OH^-$ and $Co^{2+} + 2OH^- \rightarrow Co(OH)_2$.

3.2 Optimization of deposition time

The effect of deposition time on the synthesis of nanosized $Co(OH)_2$ was investigated from 100 s to 500 s, and Fig.2 displayed cyclic voltammetric curves of $Co(OH)_2$/3DGR/CILE in the 1.0 mol/L KOH solution with different electrodeposition time. It can be seen that the maximum area of cyclic voltammogram was obtained at 300 s, indicating the biggest capacitance value. With the increase of deposition time from 100 s to 300 s, more nanosized $Co(OH)_2$ could be formed on the surface of 3DGR gradually with the capacitance increased. However, when the deposition time was more than 300 s, the $Co(OH)_2$ layers on 3DGR were too thicker and not benefit for the electron transfer with the capacitance value decreased [30]. Therefore at the electrodeposition time of 300 s the formed $Co(OH)_2$/3DGR composite exhibited synergetic effects with the maximum specific capacitance, which was selected as the optimal deposition time.

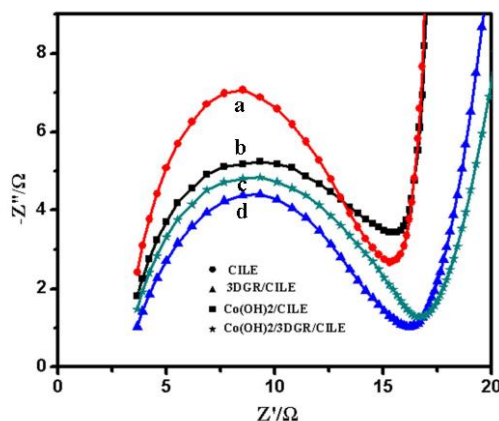**Figure 2.** Cyclic voltammetric curves of $Co(OH)_2$/3DGR/CILE prepared under different electrodeposition time (100 s, 200 s, 300 s, 400 s, 500 s) for the synthesis of nanosized $Co(OH)_2$, the supporting electrolyte is 1.0 mol/L KOH solution with the scan rate of 0.1 V/s.

3.2. Electrochemical impedance spectroscopy

Electrochemical impedance spectroscopy (EIS) can provide impedance information of the modified electrodes, which were performed in a 0.1 mol/L KCl solution containing 10.0 mmol/L $[Fe(CN)_6]^{3-/4-}$ with the frequency swept from 10^4 to 10^{-1} Hz and the results were presented in Fig.3. The diameter of the semicircle usually equals to the electron transfer resistance (R_{et}). The lower Ret can reduce the energy loss of the charge and discharge process, which is important parameter to select the electrode material of the supercapacitor. The R_{et} value of CILE (curve a) was got as 15.6 Ω and that of

3DGR/CILE (curve d) gave the minimum value of 9.8 Ω, which was due to the high conductivity of 3DGR. Therefore 3DGR on the electrode surface provided a fast conductive path for charge transfer. On Co(OH)$_2$/CILE (curve b) the largest value of R$_{et}$ was got as 32.3 Ω, which could be attributed to the presence of semi-conductive Co(OH)$_2$ that hindered the electron transfer. On Co(OH)$_2$/3DGR/CILE (curve c) the Ret was got as 12.9 Ω, indicating that the presence of 3DGR effectively reduced the electron transfer resistance. Therefore the lowest R$_{et}$ value on Co(OH)$_2$/3DGR/CILE indicated that the high conductivity and low resistance of nanocomposite on the electrode surface.
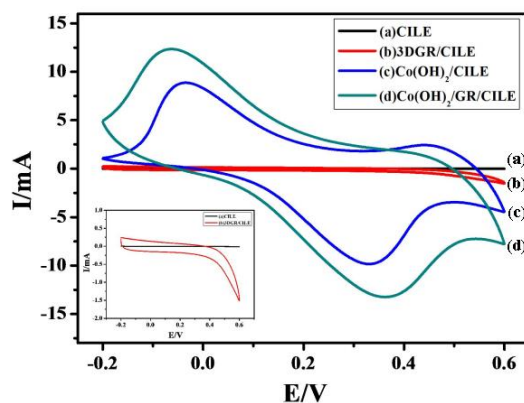

Figure 3. EIS of different modified electrodes in a 0.1 mol/L KCl solution containing 10.0 mmol/L [Fe(CN)$_6$]$^{3-/4-}$ with the frequency swept from 10^4 to 10^{-1} Hz. Electrodes: (a)CILE, (b) Co(OH)$_2$/CILE, (c) Co(OH)$_2$/3DGR/CILE and (d) 3DGR/CILE.
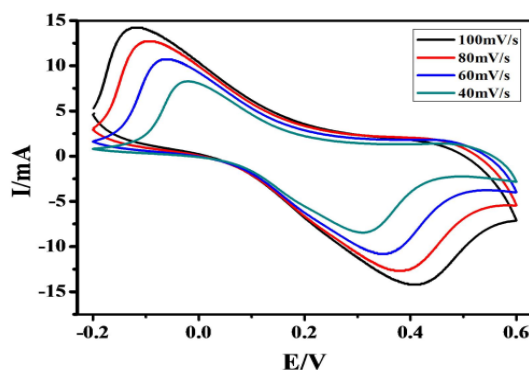
3.3. Cyclic voltammetric behaviors

Cyclic voltammograms of different modified electrodes in a 1.0 mol/L KOH solution were recorded and shown in Fig.4. On CILE (curve a) a couple of straight line appeared with the smallest area. The area was significantly increased on 3DGR/CILE (curve b) as compared with that of CILE (curve a), indicating that the presence of 3DGR on the electrode surface exhibited electrical double-layer capacitance due to its porous and layered structure [31]. The interconnected GR nanosheets resulted in the formation of 3DGR, and the double layer capacitance between GR nanosheet were present and increased with 3D porous structure. On Co(OH)$_2$/CILE (curve c) and Co(OH)$_2$/3DGR/CILE (curve d) a pair of redox peaks appeared with the current values increased. It was attributed to the pseudocapacitive Co(OH)$_2$ nanomaterial that improved the supercapacitor performance [32]. In the alkaline environment, there are two redox reactions of typical energy storage mechanism described with the following equations [33, 34]: Co(OH)$_2$ +OH$^-$$\leftrightarrow$ CoOOH + H$_2$O + e$^-$ and CoOOH + OH$^-$ $\leftrightarrow$ CoO$_2$ + H$_2$O + e$^-$. On Co(OH)$_2$/3DGR/CILE and Co(OH)$_2$/CILE the appearance of a pair of redox peaks was due to two adjacent peak that were merged into a broad peak. During the charging process the electrode reaction corresponded to the oxidation of Co(OH)$_2$ to CoOOH. While at the discharging process the electrode reaction corresponded to the reduction of CoO$_2$ to CoOOH and two processes easily converted at fast sweep speed. Also the area of cyclic voltammetric curve of

Co(OH)$_2$/3DGR/CILE was larger than that of Co(OH)$_2$/CILE, indicating the synergetic effects of Co(OH)$_2$ and 3DGR to the performance of supercapacitance. 3DGR can provide more attachment sites for the electrodeposition of Co(OH)$_2$ and facilitate the electrode transfer rate between Co(OH)$_2$ and electrolyte. The ordered assembly of 3DGR and Co(OH)$_2$ nanomaterial could combine the double electric layer capacitor properties of 3DGR and the pseudocapacitance of Co(OH)$_2$ nanomaterial with the greatly improvement of bulk capacitance [35].

Figure 4. CV of (a) CILE, (b) 3DGR/CILE,(c) Co(OH)$_2$/CILE and (d) Co(OH)$_2$/3DGR/CILE in a 1.0 mol/L KOH solution with the scan rate of 0.1 V/s.

3.4. Effects of scan rates
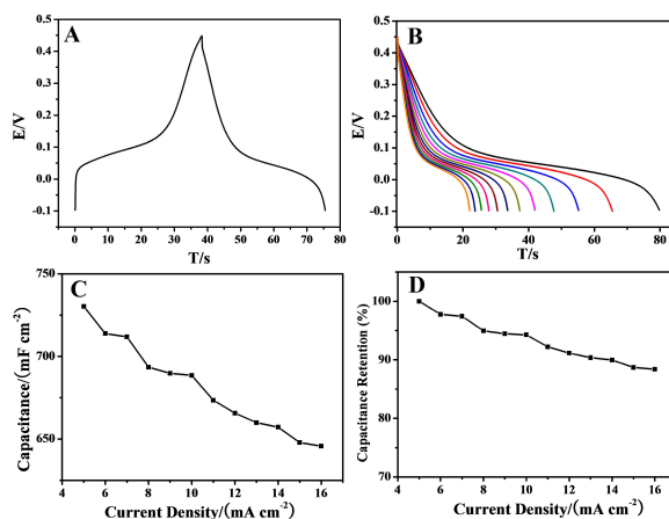

Figure 5. Influence of scan rate on cyclic voltammetric responses of Co(OH)$_2$/3DGR/CILE in a 1.0 mol/L KOH solution with the scan rates of 0.04, 0.06, 0.08, 0.1 V/s.

Fig.5 showed that the influence of scan rate on cyclic voltammetric responses of Co(OH)$_2$/3DGR/CILE in the potential window of -0.2 to 0.6 V with scan rates in the range from 40 to 100 mV/s. It can be seen that a pair of obvious redox peaks appeared, indicating a quasi-reversible electrode reaction in the charge/discharge process. Cyclic voltammetric curves had well shape at different scan rate, demonstrating that the nanocomposite exhibited an excellent electrochemical reversibility with rate capability. The redox peak currents increased gradually with scan rates and the redox peak potentials were shifted with the increase of the peak-to-peak separation, which was

attributed to the chemical reaction between $Co(OH)_2$ and OH^- in the KOH solution [36]. At higher scan rate the relaxation time of the redox reaction is limited and suppressed the effective diffusion of OH^-. Therefore the surface depth of the charge-storing $Co(OH)_2$ relatively shallow. At lower scan rate most surface active material is used completely to store charge and the diffusion of OH^- become deep, which allowed a large specific capacitance value [37, 38].

3.5. Charge and discharge investigation

The charge and discharge curve of $Co(OH)_2/3DGR/CILE$ at current density of 10 mA/cm^2 was recorded and shown in Fig.6A, which presented the obvious symmetrical plateaus characteristic. The potential plateaus in charge-discharge processes corresponded to the anodic and cathodic peaks in the CV curve, which was attributed to $Co(OH)_2/3DGR$ nanocomposite with the characteristic of Faraday pseudocapacitance [39]. The Galvanostatic current discharge curves of $Co(OH)_2/3DGR/CILE$ at different current densities from 5 mA/cm^2 to 16 mA/cm^2 were shown Fig.6B. With the increase of the discharge current density, discharge time of $Co(OH)_2/3DGR/CILE$ decreased gradually (Fig.6C). The specific capacitance can be calculated according to the following equation [40]: $C = \dfrac{I\Delta t}{S\Delta V}$, where C (F/cm^2) is the specific capacitance, I (mA) the the discharge current, Δt (s) the discharge time, ΔV (V) represents the potential drop and the area of electrodeS (cm^2) , respectively. Based on above equation, the values of specific capacitance for $Co(OH)_2/3DGR$ was calculated as 730.23 mF/cm^2 at the discharge current density of 5 mA/cm^2 and 645.66 mF/cm^2 at the current density of 16 mA/cm^2.

Figure 6. (A) Galvanostatic charge-discharge curves of $Co(OH)_2/3DGR/CILE$ at current density 10 mA/cm^2; (B) Galvanostatic discharge curves at different current densities (5 mA/cm^2-16 mA/cm^2); (C) The relationship of capacitance versus current density; (D) The relationship of capacitance retention versus current density.

The changes could be attributed to the following reasons: (1) the adsorption of OH^- was increased on the electrode surface in a short period of time with a large current density of charge

process, which caused the decrease of OH^- concentration between electrode and electrolyte, then increased the polarization phenomenon by liquid phase diffusion on the surface of electrode. Therefore the specific capacitance decreased with the potential increased. (2) at large current density, OH^- was easily reacted with $Co(OH)_2$/3DGR nanocomposite presented on the surface and was difficult to enter inside of nanocomposite, which caused the loss of specific capacitance.

Fig.6D showed capacitance retention versus current density, which indicated that capacitance still retained 88.42% with current density increased from 5 mA/cm^2 to 16 mA/cm^2. Therefore $Co(OH)_2$/3DGR nanocomposite had good electrochemical stability and reversibility. When the charge and discharge were performed under the large current density, large specific surface and three-dimensional structure made $Co(OH)_2$ fully contact with the electrolyte, which accelerated charge and discharge reaction at high current density with good capacity value resulted. The specific capacitance value of $Co(OH)_2$/3DGR was compared with other literatures and showed in Table 1. The specific capacitance value of $Co(OH)_2$/3DG was higher than porous graphene networks/nickel foam (183.2 mF/cm^2) and three-dimensional graphene oxide/polypyrrole (387.6 mF/cm^2) [41,42], respectively. More comparisons with other literatures could be observed with different electrode materials in table 1.
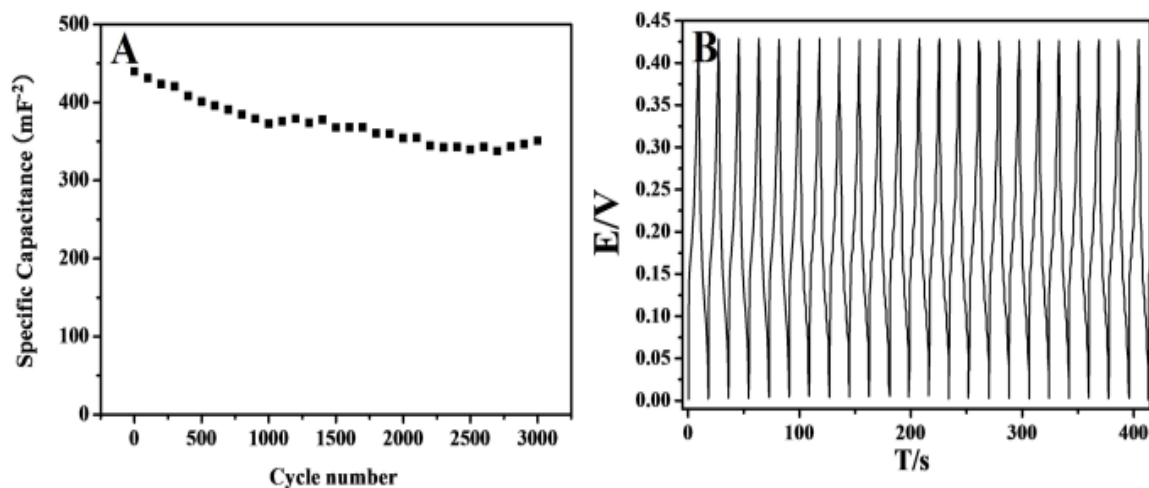
Table 1. Comparison of specific capacitance of different electrode materials

Electrode materials	Electrolyte	Specific capacitance	Current density (mA/cm^2)	References
Porous graphene Networks	6 mol/L KOH	183.2 mF/cm^2	1	[41]
Three-dimensional graphene oxide/polypyrrole	1 mol/L KCl	387.6 mF/cm^2	0.2	[42]
Reduced graphene oxide sheets/polyaniline nanofibers	0.1mol/L Aniline/1mol/L H_2SO_4	5.16 F/cm^2	10	[15]
Hierarchical mesoporous graphene and ternary nickel cobalt sulfide arrays	6mol/L KOH	9.2 F/cm^2	100	[40]
$Co(OH)_2$/3DGR	1 mol/L KOH	730.23mF/cm^2	5	This work

3.6. Charge and discharge cyclic stability of Co(OH)$_2$/3DGR/CILE

Charge and discharge cyclic stability test, which is an important parameter for supercapacitive electrodes, was carried out at current density of 20 mA/cm^2 for 3000 cycles [43]. The results of specific capacitance and number of charge–discharge cycles were shown in Fig.7A with partial detail of charge-discharge curves exhibited in Fig.7B. The initial specific capacitance of $Co(OH)_2$/3DGR nanocomposite was 439.81 mF/cm^2 and was decreased to 351.12 mF/cm^2 after 3000 cycles, which exhibited pseudocapacitance retention with 79.83 % maintenance. Therefore $Co(OH)_2$/3DGR/CILE

exhibited relatively stable electrochemical performances in the cyclic test.

Figure 7.(A) Cycling stability test at current density of 20 mA/cm^2 and (B) the partial of charge-discharge curves

4. CONCLUSION

In summary Co(OH)$_2$/3DGR nanocomposite was easily synthesized on the CILE surface by directly electrodeposition, which gave a three-dimensional disordered porous network that could greatly increase the contact area between material and electrolyte. Excellent capacitance performance could be observed on Co(OH)$_2$/3DGR modified electrode with its electrochemical performances checked by various methods such as cyclic voltammetry, electrochemical impedance spectroscopy, galvanostatic current charge and discharge method. At the current density of 5 mA/cm^2, specific capacitance was got as 730.23 mF/cm^2, which was better than some references results. The specific capacitance retained 79.83% after 3000 cycles at a current density of 20 mA/cm^2, which illustrated that Co(OH)$_2$/3DGR composite colud act as an ideal supercapacitor electrode materials.

References

1. G. V. Lier, C. V. Alsenoy, V. V. Doren, P. Geerlings, *Chem. Phys. Lett.*, 326 (2000) 181.
2. A. H. Castro Neto, F. Guinea, N. M. R. Peres, K. S. Novoselov, A. K. Geim, *Rev. Mod. Phys.*, 81 (2009) 109.
3. J. Kim, J. Oh, C. In, Y. S. Lee, T. B. Norris, S. C. Jun, H. Choi, *Acs Nano*, 8 (2014) 2486.

4.　C. G. Liu, Z. N. Yu, D. Neff, A. Zhamu, B. Z. Jang, *Nano lett.*, 10 (2010) 4863.

5.　L. L. Zhang, R. Zhou, X. S. Zhao, *J. Mater. Chem.*, 20 (2010) 5983.

6.　Z. S. Wu, Y. Sun, Y. Z. Tan, S. Yang, X. Feng, K. Müllen, *J. Am. Chem. Soc.*, 134 (2012) 19532.

7.　Y. M. He, W. J. Chen, X. D. Li, Z. X. Zhang, J. C. Fu, C. H. Zhao, and E. Q. Xie*, Acs Nano*, 7 (2013) 174.

8.　X. H. Cao, Y. M. Shi, W. H. Shi, X. H. Rui, Q. Y. Yan, J. Kong, H. Zhang, *Small,* 9 (2013) 3433.

9.　C. M. Zhao, X. Wang, S. M. Wang, Y. Y. Wang, Y. X. Zhao, W. T. Zheng, *Int. J. Hydrogen Energy*, 37 (2012) 11846.

10. Y. S. Yun, H. H. Park, H. J. Jin, *Materials*, 5 (2012) 1258.

11. S. Li, P. Xue, C. Lai, J. X. Qiu, M. Ling, S. Q. Zhang, *Electrochim. Acta*, 180 (2015) 112.

12. M. A. Garakani, S. Abouali, B. Zhang, Z. L. Xu, J. Huang, J. Q. Huang, *J. Mater. Chem.* A, 3 (2015) 17827.

13. D. Sacer, M. Kralj, S. Sopcic, M. Kosevic, A. Dekanski, M. R. Kraljic, *J. Serb. Chem. Soc.*, 82 (2017) 411.

14. U. Patil, S. C. Lee, S. Kulkarni, J. S. Sohn, M. S. Nam, S. Han, S. C. Jun, *Nanoscale,*7 (2015) 6999.

15. Z. Gao, W. L.Yang, J. Wang, H. J.Yan , Y. Yao, J. Ma, B. Wang, M. L. Zhang, L. H. Liu. *Electrochim. Acta,* 91 (2013) 185.

16. Q. Q. Zhang, Y. Li, Y. Y. Feng, W. Feng, *Electrochim. Acta*, 90 (2013) 95.

17. J. Yan, Z. J. Fan, T. Wei, W. Z. Qian, M. L. Zhang, F. Wei, *Carbon*, 48 (2010) 3825.

18. S. Chen, J. W. Zhu, X. Wang, *J. Phys. Chem*. C, 114 (2010) 11829.

19. X. H. Xia, J. P. Tu, Y. Q. Zhang, Y. J. Mai, X. L. Wang, C. D. Gu, X. B. Zhao, *J. Phys. Chem*. C, 115 (2011) 22662.

20. J. K. Chang, C. M. Wu, I. W. Sun, *J. Mater. Chem*., 20 (2010) 3729.

21. L. Wang, Z. H. Dong, Z. G. Wang, F. X. Zhang, J. Jin, *Adv. Funct. Mater*., 23 (2013) 2758.

22. A. Jabbar, G. Yasin, W. Q. Khan, M. Y. Anwar, R. M. Korai, M. N. Nizamb, G. Muhyodin, *Rsc Adv*., 7 (2017) 31100.

23. C. Z. Zhu, S. J. Guo, Y. X. Fang, S. J. Dong, *ACS Nano*, 4 (2010) 2429.

24. F. Shi, J. W. Xi, F. Hou, L. Han, G. J Li, S. X. Gong, W. Sun, *Mater. Sci. Eng.* C, 58 (2016) 450.

25. Y. Y. Shao, J. Wang, M. Engelhard, C. M. Wang, Y. H. Lin, *J. Mater. Chem.*, 20 (2010) 743.

26. S.Y. Toh, K.S. Loh, S.K. Kamarudin, W.R.W. Daud, *Chem. Eng. J.*, 251 (2014) 422.

27. M. Yu, Y.X. Ma, J.H. Liu, S.M. Li, *Carbon*, 87 (2015) 98.

28. M. Mirzaee, C. Dehghanian, K. S. Bokati, *J. Electroanal. Chem*., 813 (2018) 152.

29.W.J. Zhou, J. Zhang, T. Xue, D.D. Zhao, H.L. Li, *J. Mater. Chem.* A,18 (2008) 905.

30. Q. Xie, X. Chen, H.M. Liu, W.S. Yang, *Sens. Actuators,* B, 168 (2012) 277.

31. W. Tang, L. Peng, C.Q. Yuan, J. Wang , S.B. Mo, C.Y. Zhao ,Y.H. Yu , Y.G. Min, *Synth. Met*., 202 (2015) 140.

32. L. Cao, F. Xu, Y.Y. Liang, H.L. Li, *Adv. Mater*.,16 (2004) 1853.

33.C. M. Wu, C. Y. Fan, I. W. Sun, W. T. Tsai, J. K. Chang, *J. Power Sources*, 196 (2011) 7828.

34.J. Jiang, J. Q. Liu, R. M. Ding, J. H. Zhu, Y. Y. Li, A. Z. Hu, X. Li, X. T. Huang. *ACS appl. Mater. Inter.*, 3 (2011) 99.

35. D. Ghosh, S. Giri, C. K. Das, *ACS Sustainable Chem. Eng*., 1 (2013) 1135.

36. A.D. Jagadale, V.S. Kumbhar, D.S. Dhawale, C.D. Lokhande. *Electrochim. Acta*, 98 (2013) 32.

37. T. Xue, X. Wang, J.M. Lee. *J. Power Sources*, 201 (2012) 382.

38. F. Cao, G.X. Pan, P.S. Tang, H.F. Chen. *J. Power Sources*, 216 (2012) 395.

39. H.W. Wang, H. T. Tan, H. Yi, Y. Zhang, G.L. Guo, X.F. Wang, S. Madhavi and Q.Y. Yan, *Rsc Adv*., 5 (2015) 88191.

40. V. H. Nguyen, C. Lamiel, J.J. Shim, *Electrochim. Acta*, 161 (2015) 351-357.

41. S.L. Yang, B.C. Deng, R.J. Ge, L. Zhang, H. Wang, Z.H. Zhang, W. Zhu, G.Z. Wang, *Nanoscale Res. Let*., 9 (2014) 2496.

42. J.Y. Cao, Y.M. Wang, J.C. Chen, X.H. Li, F. C. Walshc, J.H. Ouyanga, D. Jia, Y. Zhou, *J. Mater. Chem.* A, 3 (2015) 14445.
43. Z.J. Fan , J. Yan, T. Wei, L.J. Zhi, G.Q. Ning, T.Y. Li and F. Wei, *Adv. Funct. Mater.*, 21 (2011) 2366.